A short course of antibiotics selects for persistent resistance in the human gut

Eitan Yaffe[1,3]*, Les Dethlefsen[1], Arati V. Patankar[3], Chen Gui[3], Susan Holmes[4], David A. Relman[1,2,3]

[1]Department of Medicine, Stanford University School of Medicine; Stanford, CA USA.

[2]Department of Microbiology and Immunology, Stanford University School of Medicine; Stanford, CA USA.

[3]Infectious Diseases Section, Veteran Affairs Palo Alto Health Care System; Palo Alto, CA USA.

[4]Department of Statistics, Stanford University, Stanford; CA USA.

*Corresponding author. Email eitan.yaffe@stanford.edu

Understanding the relationship between antibiotic use and the evolution of antimicrobial resistance is vital for effective antibiotic stewardship, yet animal models and *in vitro* experiments poorly replicate real-world conditions. To elucidate how resistance evolves in the human gut, we exposed 60 human subjects to ciprofloxacin and used longitudinal stool samples and a new computational method to assemble genomes for 5665 populations of bacterial species within subjects. Analysis of 2.27M polymorphic sequence variants revealed 513 populations that underwent selective sweeps, with over 65% of sweeping variants persisting more than 10 weeks. We found 65 cases of convergent evolution involving DNA gyrase and evidence of selective pressure at other genomic loci. Evolutionary trajectories towards ciprofloxacin resistance were shaped by population abundances before and during the exposure. This work quantifies the relationship between antibiotic usage and the evolution of resistance within the gut communities of individual human hosts.

INTRODUCTION

Antimicrobial resistance (AMR) is an growing global health threat, projected to cause millions of deaths worldwide by 2050 (*1*, *2*). AMR is driven by the overuse and misuse of antibiotics (*3*), and is associated with geographic factors (*4*) and seasonal patterns (*5*). AMR is not limited to heavily prescribed patients and is instead linked to low-intensity outpatient antibiotic usage (*6*). Prescription data suggest that AMR primarily evolves due to bystander selective pressure, where colonizing pathogens evolve resistance subclinically in patients taking antibiotics for unrelated problems (*7*). However, the evolution of AMR *in vivo* is rarely documented; instead, resistant pathogens usually emerge in infections after evolving elsewhere, as seen with resistant *Escherichia coli* associated with urinary tract infections (*8*) and surgical site infections (*9*). In contrast to the sparsity of data directly from treated human subjects, the evolution of AMR has been extensively studied *in vitro* (*10*–*16*) and using animal models (*17*, *18*). Yet, these laboratory experiments struggle to reproduce clinical conditions faithfully, most of which are poorly understood, including local drug concentrations that vary in time and space, microbial population sizes, the effects of immune system responses, and interactions within microbial communities (*19*–*23*). Quantifying the evolution of AMR in clinically relevant settings can provide new opportunities for combatting AMR by informing antibiotic stewardship and developing personalized antibiotic treatments.

Fluoroquinolones are a class of potent broad-spectrum antibiotics that make up a fifth of global antibiotic consumption (*24*). In contrast to the majority of antibiotics for which horizontal gene transfer plays an important role in the evolution of resistance (*25*, *26*), fluoroquinolone resistance (FQR) primarily involves mutations in the drug targets (Type II topoisomerases) with mobilized genes playing only a supporting role (*27*, *28*). Analysis of pathogen genomes and *in vitro* experiments suggest that FQR evolves through a stepwise process that begins with specific mutations in DNA gyrase and topoisomerase IV (*14*, *29*–*31*). However, the specific conditions under which these mutational processes occur in real-world settings remain poorly understood.

Commensal evolution in the gut of adults is evident over a timeframe of several years (*32*–*35*), and over shorter timeframes during the use of antibiotics (*36*), after fecal microbiota transplantation (*37*), or in newborns (*38*). Fluoroquinolone concentrations in the human gut are high and persist days after oral treatment (*39*), exerting a strong selective pressure (*40*), and disrupting gut communities (*41*). We therefore hypothesized that gut commensals would evolve resistance during a single, brief course of ciprofloxacin, allowing us to quantify key aspects of the evolution of AMR *in vivo*.

From a technical perspective, studying *in vivo* evolution in natural settings is challenging. The microbial communities within a single human gut are composed of hundreds of localized populations, each founded through one or several rounds of colonization (*34*, *42*). Gene duplications and horizontal gene transfer result in a convoluted genomic landscape riddled with sequence homology between genomes, resulting in non-trivial relationships between genomes and genome assemblies (*35*). One powerful genotyping approach is to sample a community repeatedly over time, which permits sequences to be associated and assembled based on their co-abundance across samples. Dense longitudinal sampling has been used to resolve genomes

(*43–45*) and microbial strains (*36*, *46–48*). However, existing strain recovery tools utilize heuristic approaches to identify true polymorphic sites, which are often embedded in a background of spurious variant sites that may arise during genome assembly due to sequence homology within and between genomes. As of now, there is no method that effectively leverages dense longitudinal sampling to assemble genomes and accurately identify true polymorphic sites.

In this study, we exposed 60 subjects to a fluoroquinolone antibiotic, ciprofloxacin, orally for five days and collected longitudinal stool samples before and after exposure for a period of 20 weeks to study how gut commensals evolve under antibiotic selective pressure *in vivo*. To identify underlying polymorphisms, we developed a tool (PolyPanner) that simultaneously reconstructed 5665 genomes of localized populations of species and their 2.27M polymorphic variants. PolyPanner is unique in its ability to leverage the statistical power of longitudinal shotgun metagenomic data to enrich for true polymorphic sites. Analysis of variants that swept in an antibiotic-associated manner uncovered evidence of convergent evolution focused on a pair of amino acids within the gene that encodes DNA gyrase subunit A, *gyrA*, alongside evidence of dispersed selective pressure elsewhere. The probability of selective sweeps involving mutations in *gyrA* was strongly influenced by population abundances both before and during antibiotic exposure, with potential clinical implications. This study provides valuable insights into the relationship between antibiotic usage and the evolution of resistance in human associated microbiotas.

RESULTS

Sixty healthy adult volunteers took a short course of ciprofloxacin (500mg orally, twice daily, 5 days) and self-collected 16 stool samples over a period of 20 weeks including daily sampling before, during and after the antibiotic exposure (960 samples in total, see **Supp. Fig. S1**). Stool-derived DNA libraries from all 960 samples were sequenced with 18.8M (million) reads per sample on average. We processed the temporal shotgun reads to generate metagenome-assembled genomes (MAGs) and their polymorphic sites using PolyPanner, a program developed here and described in **Methods** (see **Supp. Fig. S2** for an overview of the workflow).

Reads were pooled within subjects to generate 60 subject-specific metagenome co-assemblies spanning ~400Mb on average. For each sample, reads were aligned to their respective subject assembly, generating single-nucleotide coverage profiles which represent fluctuations in the abundance of all assembled base pairs over the 16 time points. Chimeric contigs were segmented by applying an algorithm that located abrupt transitions in coverage profiles along contigs (**Methods**). These transitions are likely chimeric assembly breakpoints where the two sides of the breakpoint represent different populations and confound downstream analysis. When applied to our dataset, the algorithm identified ~10k such breakpoints (involving 2.1% of contigs) per subject on average. Contigs were segmented on these breakpoints and the resulting segments were binned (i.e., clustered) into metagenomic assembled genomes (MAGs), based on average segment-level coverage profiles, resulting in 109k genome bins per subject on average. Downstream analysis was limited to 5665 genomes (51-166 genomes per subject) that were at

least 50% complete and not more than 10% contaminated. On average, the selected genomes were 81.3% complete and 1.8% contaminated (**Supp. Figure S3**), with median sequencing depth (summed across the 16 samples per subject) of 51x (5x to 3856x). Each genome putatively represented the population of a single bacterial species inhabiting the gut of a specific subject. The 5655 populations spanned 924 distinct species, 378 genera and 81 families (**Supp. Table S1**).

Populations were disturbed yet mostly resilient to the antibiotic exposure

We examined the population-level response to the antibiotic exposure, as reflected by changes in population abundance over time. Population response trends included transient decreases and increases in abundance, indicating relative ciprofloxacin sensitivity and resistance or tolerance, as well as putative extinction events (**Fig. 1A**). During the height of the disturbance (days 3 to 8 after the start of ciprofloxacin) 15.9% of populations were below the detection limit and by day 28 10.3% of populations remained undetected and putatively extinct (**Fig. 1B**). Conversely, 0.9% of the populations were not observed at baseline and emerged during the height of the disturbance. The rank order of persistent populations was disrupted during the disturbance (Spearman rho=0.31) and returned closer to baseline by day 28 (rho=0.62). The relatively few extinction events and the overall return to baseline rank of persisting populations attested to the resilience of the human gut microbiome. Response trends were broadly associated with taxonomic identity (**Supp. Fig. S4**), yet diverse taxa such as the *Lachnospiraceae* family were highly heterogenous in their response (**Supp. Fig. S5**). The resilience of gut populations, despite the antibiotic-associated disruption, created a unique opportunity to assess how ciprofloxacin drives evolution in gut commensals.

Identifying polymorphic variants in mixed populations

We wished to identify true polymorphic sites, defined as variant sites that segregated within a single population. Mismatches in read alignments were identified on a single-nucleotide basis, resulting in variant sites typed as single nucleotide polymorphisms (SNPs), short insertions or deletions (indels), and genome rearrangement breakpoints. Sequencing errors were identified using a probabilistic approach and removed (**Methods**), resulting in 107.1 million variants. Due to genomic sequences shared between populations and duplicated genes within populations, not all variants inferred in this manner reflected true polymorphic variants (**Supp. Fig. S6**). We developed an approach to enrich for what we call *dynamic variants*, which are polymorphic variants with a non-constant frequency over time, after taking into account read sampling stochasticity (see **Methods** for details). The remaining variants, which we call *spurious variants*, reflect either homology between distinct populations (*ortholog variants*) or homology within a population due to duplicated genes (*paralog variants*), and were considered noise for our purpose of tracking competing alleles within a single bacterial population. To our knowledge, this approach is the first explicit modelling and classification of variant types and allows one to enrich for true polymorphic variants using longitudinal shotgun data.

We assessed the density of spurious variants and benchmarked our ability to remove them by simulating data from 100 bacterial communities with different numbers of introduced dynamic variants (40G paired reads in total). Spurious variants were pervasive, with typically 50-150

spurious variants per Mb of genome, even when few mutations were simulated (**Supp. Fig. S7A**). With our approach, the fraction of spurious variants that were misclassified as dynamic was less than 0.3%, regardless of sequencing depth, meaning that our approach enriched dynamic variants by over 100-fold. Sensitivity depended on the sequencing depth and the mutation type. Local mutations (SNPs and indels) began to be detected at a sequencing coverage threshold of 50x per genome and plateaued at 60-80% of variants detected (failing to reach 100% due to incomplete genome assemblies) when coverage was above 100x (**Supp. Fig. S7B**). The sensitivity of detection for large-scale genome rearrangements was lower (**Supp. Fig. S7C**). Importantly, the precision remained high in the face of "genetic crowding" in which communities contained multiple members of the same genus or family (**Supp. Fig. S8**). Taken together, simulated data demonstrated the pervasiveness of spurious variants and showed that our approach is well-suited to detect dynamic variants in evolving bacterial communities.

Hundreds of populations underwent putative selective sweeps

Application of our approach to the 5665 populations resulted in 2.27 million dynamic variants, making up 2.1% of all variants ("Genome" table in **Supp. Table S1**). Dynamic variants were comprised of 98.5% SNPs, 1.3% indels and 0.2% rearrangement breakpoints. Dynamic variants were found in 2133 populations (37.6%), yet the size of this fraction was dependent on sequencing depth, as the percentage of populations with dynamic variants among sufficiently sequenced populations (with an abundance above ~1%) was 85.8% (**Fig. 2A**). We limited the analysis to 1866 populations that had 1-1000 dynamic variants, omitting 267 populations with over 1000 variants that were composed of distant conspecific strains. Underlying strain genomes and their temporal trajectories were approximated using a probabilistic model (*47*), resulting in 2-8 strains per population (**Fig. 2B**). For each population, strains were arranged on a most-parsimonious phylogenetic tree, and each tree branch was associated with a *linkage group* (LG), defined as the set of variants that were inferred to change along the branch. We considered the LG size a crude estimator of the mean age of the variants in the linkage group, where small linkage groups indicated recent events (including *de novo* mutations and recombination events), and large groups earlier events. Smaller LGs were correlated with elevated levels of non-synonymous mutations, measured using dN/dS ratios (**Fig. 2C**). There were 7132 variants that "swept" from a pre-antibiotic frequency below 20% to over 80% post-antibiotic ("Variant" table in **Supp. Table S2**). Each sweeping variant represented a putative mutation that transitioned from the baseline to the post-exposure variant state. Sweeping variants involved 513 populations that were distributed across all subjects (8.55 ± 4.15 populations per subject) and involved 212 species (22.9% of species). Sweeping variants rarely traveled alone: only 1% were the only member in their LG and 6.5% had 2-10 variants in their LG (**Supp. Fig. S9**). We illustrate how variants are organized into strains and linkage groups using a *Alistipes putredinis* population found in subject EBW, where an antibiotic-associated shift in strain composition could be attributed to an LG composed of 2 mutations, one of which was in the gyrase subunit A (*gyrA*) (**Fig. 2D**).

Convergent evolution focused on gyrA

A strain can sweep following antibiotic exposure because it carries an adaptive 'driver' mutation, but additional 'passenger' variants in the same strain may also be swept to high abundance (*49*). We therefore searched for evidence of evolution occurring in parallel in different populations and subjects. To reduce the background noise of passenger variants, we focused our analysis further on 1771 sweeping variants (in 312 populations) that were part of small LGs (up to 100 variants/LG). Variants were associated with single genes if intragenic or with two adjacent genes if intergenic. Interestingly, 22.5% of implicated genes were associated with multiple variants in the same population, indicating that at least some of the genetic variation was likely introduced through recombination (**Supp. Fig. S10**). Genes were annotated using the KEGG Orthology (KO) database, with special attention to distinguishing between the homolog genes, gyrase subunit A (*gyrA*, K02469) and topoisomerase IV subunit A (*parC*, K02621) (*50*, *51*) (**Supp. Fig. S11** and **Supp. Table S3**). Variants were assigned a weight inverse to the size of their LG, and weights were aggregated within KOs, resulting in 803 KOs with positive weights. Weight enrichment ratios were computed over a background model in which variants were randomly reassigned to a gene within their genome, resulting in 20 significant KOs that showed evidence of convergent evolution (**Supp. Fig. S12** and **Supp. Table S4**). The top hit in terms of fold-enrichment and statistical significance was *gyrA* (68 variants, 373-fold enrichment, $P < 1.25 \times 10^{-5}$) (**Fig. 2E**). *GyrA* sweeps occurred in 63 populations inhabiting 34 subjects. A dN/dS ratio of 3.9 and a median LG size of 2 were highly suggestive that *gyrA* mutations occurred *de novo* within the gut of the subjects (**Fig. 2F**). See **Supp. Fig. S13** for examples of *gyrA*-associated sweeps.

Beyond *gyrA*, the selective pressure was less focused and was distributed among the remaining 19 KOs, with no single KO involving more than 6 populations. Breakdown of KOs by taxonomic identity showed how *gyrA* sweeps were widely distributed (41 species, 15 families), while other KOs were typically limited to specific taxa (**Supp. Fig. S14**). Notably, *parC* was enriched in mutations yet to a lesser degree (5 variants in 3 families) than its close homolog *gyrA* (68 variants), possibly because of reduced selective pressure due to its distinct role compared to DNA gyrase (*52*), and in contrast to previous findings suggesting that Gram positive bacteria evolve primarily through mutations in *parC* (*27*). Other implicated KOs included efflux pumps (K02004), DNA helicases (K02314, K03657), transport systems (K01537, K02051, K11085), transcription factors (K19505) and phage-associated genes (K01421). The inhibition of the helicase DnaB (K02314) has been implicated previously in FQR in *E. coli* (*53*). While parallel evolution beyond *gyrA* was limited, there were compelling examples of idiosyncratic sweeps that were not driven by *gyrA* (**Supp. Fig. S15**).

Selective pressure targets specific amino acids within gyrA

The mutations associated with *gyrA* occurred mostly at two residues: *gyrA*:83 (56 substitutions) and *gyrA*:87 (9 substitutions) (*E. coli* numbering) (**Fig. 3A**). Substitutions of these two residues alone accounted for 87% of *gyrA* mutations. Substitutions at *gyrA*:83 were mainly serine to phenylalanine (S83F, 21 cases) and serine to leucine (S83L, 19 cases) (**Fig. 3B**). Substitutions at *gyrA*:83 and *gyrA*:87 are well-documented as initial steps towards fluoroquinolone resistance in a variety of pathogens and model organisms (*28*). We further focused on *gyrA*:83, which was

common in our study, occurring in 33 subjects and in 38 species that spanned 11 taxonomic families. To assess substitution probabilities, we computed the pre-disturbance baseline standing variation at *gyrA*:83 for 3896 genomes in which *gyrA*:83 could be resolved. Serine, associated with fluoroquinolone susceptibility in our study and in the literature (*14*), was present at baseline in 61.1% of genomes, while leucine and phenylalanine, associated with fluoroquinolone resistance, were present in 6% of the genomes (**Fig. 3C**). Baseline amino acids at *gyrA*:83 were associated with taxonomic identity (**Supp. Fig. S16**). The probability of an antibiotic-associated serine substitution was 9.6±1.5% per population (**Fig. 3D**). To our knowledge this is the first estimation of the rate at which ciprofloxacin resistance emerges in human subjects.

Resistance mutations at *gyrA*:87 appeared less favorable. There were only 9 such instances in total, and *Alistipes putredinis* accounted for five E87K mutations that likely occurred because these genomes have an unusual initial serine codon at *gyrA*:83 (AGU) that would require two mutations to reach the more favorable leucine or phenylalanine at position 83. Clinical isolates of *Neisseria gonorrhoeae* were recently shown to gain resistance through mutations in *gyrA*:87, while keeping serine at *gyrA*:83 (*54*).

Evidence for pre-existing resistance

We wished to leverage the large scope of the dataset to assess the prevalence of FQR prior to ciprofloxacin exposure in our subjects. We determined 40 species-specific resistance alleles at *gyrA*:83, based on the identity of the substituting amino acid in sweeping variants. Remarkably, resistance alleles were observed prior to the ciprofloxacin exposure in 26 out of 38 species (**Supp. Fig. S17**). For example, the resistance allele of *Phocaeicola vulgatus* was phenylalanine (based on 2 sweeps with S83F), and there were 15 out of 34 populations with phenylalanine at *gyrA*:83 before the exposure. Frequencies of resistant strains at baseline varied among species, ranging between 0% to 71% and averaging 33.8% (**Fig. 3E**). Of note, some species had a signature of pre-exposure resistance (based on phenylalanine or leucine at position 83), despite not having any observed sweeps in our study. For example, the percentage of resistant *E. coli* strains was estimated to be 41% at baseline (based on 5 leucines and 7 serines at *gyrA*:83), without any *gyrA* associated sweeps in *E. coli* populations. Subjects did not have significant differences in the overall level of pre-existing resistance, suggesting that most strains were likely resistant prior to colonization, rather than evolving resistance *in situ* within subjects (**Supp. Fig. S18**).

Evolvability of resistance predicted by population size and drug sensitivity

An important question with possible clinical implications is what determines the evolvability of a population when challenged with ciprofloxacin, which is the probability of a population having one or more sweeping variants. For this analysis we focused on 410 populations (out of 5665) that had serine at *gyrA*:83 at baseline and had sufficient coverage for detection of sweeps, if present (equivalent to an abundance over ~1%, as shown in Figure 2A). The overall evolvability was 0.26 based on 106 populations with one or more sweep. *GyrA* evolvability (where at least one sweep involves *gyrA*) was 0.11, based on 45 populations. Thus, *gyrA* evolution accounted for only 36% of the overall evolvability, highlighting the putative role of alternative evolutionary

trajectories in response to antibiotics. We employed logistic regression to assess whether abundance and taxonomic identity can serve as reliable predictors for the *gyrA* evolvability of a population (**Sup. Figure S19**). Logistic regression identified four significant predictors: baseline population abundance ($P<0.02$), the decline in abundance during antibiotics (average of days 1-5, $P<10^{-5}$), and phylum (Bacteroidetes $P<2x10^{-3}$ and Actinobacteria $P<2x10^{-8}$, relative to Firmicutes) (**Fig. 4A**). In terms of effect sizes, gyrA evolvability exhibited a 3.8-fold increase for every 10-fold rise in baseline population abundance and a 3.2-fold increase for every 10-fold rise in the magnitude of decline in abundance during antibiotic exposure (i.e., the ratio between abundance at baseline and during treatment). *GyrA* evolvability showed a strong association with drug sensitivity, as 90.2% of the populations that underwent a *gyrA* sweep experienced a reduction in abundance during antibiotic exposure. *GyrA* evolvability of Bacteroidetes and Actinobacteria was 3.8-fold and 26-fold higher than Firmicutes, respectively. For the most susceptible populations (i.e., with a decline of 1000-fold or more during antibiotics), evolvability equaled 0.5 when the baseline abundance was ~0.1% for Bacteroides and ~1% for Firmicutes. Model-predicted evolvability and observed evolvability were in agreement, when stratifying populations by baseline abundances (**Fig. 4B**), or by the decline in abundance during antibiotics (**Fig. 4C**).

The model performance was excellent, with an area under the curve (AUC) of 0.875 (**Fig. 4D**). Of note, a simple model that solely relies on the baseline abundance had an AUC of 0.76 and is distinctive in its capability to predict evolvability even before antibiotic exposure occurs. While differences in genus-level *gyrA* evolvability were captured by the model in general, *Collinsella* (phylum Actinobacteria) and *Lachnospira* (Firmicutes) were significantly more evolvable than predicted by the model (**Fig. 4E**). Non-*gyrA* evolvability (i.e., the probability of a sweep with a gene other than *gyrA*) was only partially explained by the abundance during antibiotics but not by the abundance at baseline and was significantly harder to predict, reaching a maximal AUC of only 0.567 (**Supp. Fig. S20**). Evolvability was not significantly different between subjects (**Supp. Fig. S21**).

The model parameters of *gyrA* evolvability are related to fundamental attributes of bacterial populations: baseline abundances are linked to absolute population sizes and the magnitude of the decline during antibiotics is a crude proxy for sensitivity to ciprofloxacin. The data and models are consistent with an enrichment of *de novo gyrA* mutations that swept primarily in populations that were both abundant and sensitive through a bottleneck event, while evolution through non-*gyrA* variants had no clear signature of *de novo* mutations, likely drew from pre-existing standing variation, and was not clearly associated with resistance.

Sweep reversion was slow

Finally, we wanted to determine the long-term effect of the exposure, by examining sweep reversions. At the time of the last sample, collected 10 weeks after the end of the exposure, 89% of *gyrA* sweeps and 65% of non-*gyrA* sweeps remained at a frequency above 80% (**Fig. 5A**). In terms of possible fixation events, 74% of *gyrA* and 56% of non-*gyrA* sweeps remained at a frequency of 100% (**Fig. 5B**). To predict the behavior beyond 10 weeks, we employed a naïve model that assumed a constant fitness cost for resistant alleles, and separately inferred selection

coefficients for all sweeps; see an example of the fastest reverting *gyrA* sweep in **Fig. 5C**. Projecting one year out, 95.1% of *gyrA* sweeps were not expected to fall below 1% frequency, which was higher than 83.8% for non-*gyrA* sweeps (P<0.029, Yates's chi-squared test). The median reversion time for sweeps that were projected to revert within a year was 109 days (**Fig. 5D**). Taken together, our data indicate that resistance mutations in *gyrA* and genetic changes at other loci can persist long after the antibiotic exposure, consistent with relatively low fitness costs or compensatory mutations.

DISCUSSION

This work describes in detail how populations of gut commensals evolve *in vivo* during and after a single short course of ciprofloxacin. We quantified, for the first time, rates at which AMR and other antibiotic-associated mutations sweep and persist in human gut communities under clinically relevant conditions. Our analysis shows that 11% of commensal populations acquire putative resistance through mutations in *gyrA*, and over 80% of acquired genetic changes remain dominant months after the antibiotic exposure. Evolvability through *gyrA* was explained by a simple model based on population abundances, with marked differences between phyla. The study reveals important processes that likely drive the evolution of ciprofloxacin resistance in humans.

Our data show that *gyrA* evolvability of bacterial populations surpasses a probability of 0.5 when population abundances cross a threshold of 0.1% and 1%, for Bacteroides and Firmicutes respectively, which together make up 86% of populations. Yet conservative assumptions (10^{13} cells in the gut, a mutation rate of 10^{-10} to 10^{-9} per bp per generation, no sweeps in the week prior to antibiotics) result in a theoretical upper bound for this threshold that ranges from 0.0002% to 0.002% (**Supp. Note 1**). The large discrepancy between theory and empirical data, and between phyla, may reflect differences in mutation rates and sweep frequencies, and can also be explained by reduced effective population sizes in the intestines due to flow (*55*). Recent *in vitro* work with *E. coli* (*14*) and *Pseudomonas aeruginosa* (*15*) showed that *gyrA* mutations sweep only when populations are large, in agreement with our *in vivo* results. The emerging picture is that large populations can evolve mutations in *gyrA* on their evolutionary trajectory towards higher levels of fluoroquinolone resistance, while smaller populations may evolve through a variety of other mutations, if at all, and are more likely to lose their resistance over time. From a clinical perspective, precise models of evolvability can inform the selection of appropriate antibiotics, as previously suggested from *in vitro* work (*31*). To give a concrete example, a clinician treating a patient with a urinary tract infection may decide against prescribing fluoroquinolones if sequencing data suggest that the abundance of a gut-residing pathogen is high enough to predict evolution of resistance during treatment. In the future, routine assessments of microbial composition and abundance could become a useful tool for mitigating risk for the patient and society (*3*).

The method presented here exploits temporal shotgun metagenomic data, allowing us to re-examine decades of *in vitro* studies and provide a more relevant understanding of how AMR evolution transpires *in vivo*. The approach is well-suited to detect adaptive evolution in diverse natural microbial communities facing selective pressure, although it has some limitations. Studying horizontal gene transfer necessitates complementary methods like Hi-C (*35*, *56*) and long-reads (*36*, *57–59*). Additionally, the method is limited in its ability to detect 'soft' sweeps in which multiple independent mutations sweep simultaneously (*60*). Such phenomena, supported by *in vitro* data (*14*), could play a significant role in the evolution of antimicrobial resistance.

The slow post-exposure loss of *gyrA* mutations may suggest that they have little or no fitness cost, a well-known concern (*27*, *61*). For example, *in vitro* experiments showed that replacing serine at *gyrA*:83 had no measurable fitness cost in *E. coli* and *Streptococcus pneumoniae* (*62*), or even conferred a fitness advantage in pathogens such as *Salmonella* Typhi and *Campylobacter jejuni* (*63*, *64*). For mutations to revert, their fitness cost must supersede the nominal selective pressure in the gut for a substantial length of time, yet the breadth of selective pressures under natural conditions (other than antibiotics) remains poorly understood.

This approach can be used to understand the evolution of resistance *in vivo* with different antibiotic classes, dosages, and durations, as well as previously unrecognized effects of other drugs and conditions that impose selective pressure on the microbiome. The results of such studies may inform the design of revised antibiotic regimens that better optimize benefit/cost ratios (*22*, *65*). By studying microbial communities in their natural environment, the net effect of myriad interacting externalities on the evolution of community members can be distilled and eventually understood.

REFERENCES

1. S. Harbarth, M. H. Samore, Antimicrobial Resistance Determinants and Future Control. *Emerg. Infect. Dis.* **11**, 794–801 (2005).

2. C. J. Murray, K. S. Ikuta, F. Sharara, L. Swetschinski, G. Robles Aguilar, A. Gray, C. Han, C. Bisignano, P. Rao, E. Wool, S. C. Johnson, A. J. Browne, M. G. Chipeta, F. Fell, S. Hackett, G. Haines-Woodhouse, B. H. Kashef Hamadani, E. A. P. Kumaran, B. McManigal, R. Agarwal, S. Akech, S. Albertson, J. Amuasi, J. Andrews, A. Aravkin, E. Ashley, F. Bailey, S. Baker, B. Basnyat, A. Bekker, R. Bender, A. Bethou, J. Bielicki, S. Boonkasidecha, J. Bukosia, C. Carvalheiro, C. Castañeda-Orjuela, V. Chansamouth, S. Chaurasia, S. Chiurchiù, F. Chowdhury, A. J. Cook, B. Cooper, T. R. Cressey, E. Criollo-Mora, M. Cunningham, S. Darboe, N. P. J. Day, M. De Luca, K. Dokova, A. Dramowski, S. J. Dunachie, T. Eckmanns, D. Eibach, A. Emami, N. Feasey, N. Fisher-Pearson, K. Forrest, D. Garrett, P. Gastmeier, A. Z. Giref, R. C. Greer, V. Gupta, S. Haller, A. Haselbeck, S. I. Hay, M. Holm, S. Hopkins, K. C. Iregbu, J. Jacobs, D. Jarovsky, F. Javanmardi, M. Khorana, N. Kissoon, E. Kobeissi, T. Kostyanev, F. Krapp, R. Krumkamp, A. Kumar, H. H. Kyu, C. Lim, D. Limmathurotsakul, M. J. Loftus, M. Lunn, J. Ma, N. Mturi, T. Munera-Huertas, P. Musicha, M. M. Mussi-Pinhata, T. Nakamura, R. Nanavati, S. Nangia, P. Newton, C. Ngoun, A. Novotney, D. Nwakanma, C. W.

Obiero, A. Olivas-Martinez, P. Olliaro, E. Ooko, E. Ortiz-Brizuela, A. Y. Peleg, C. Perrone, N. Plakkal, A. Ponce-de-Leon, M. Raad, T. Ramdin, A. Riddell, T. Roberts, J. V. Robotham, A. Roca, K. E. Rudd, N. Russell, J. Schnall, J. A. G. Scott, M. Shivamallappa, J. Sifuentes-Osornio, N. Steenkeste, A. J. Stewardson, T. Stoeva, N. Tasak, A. Thaiprakong, G. Thwaites, C. Turner, P. Turner, H. R. van Doorn, S. Velaphi, A. Vongpradith, H. Vu, T. Walsh, S. Waner, T. Wangrangsimakul, T. Wozniak, P. Zheng, B. Sartorius, A. D. Lopez, A. Stergachis, C. Moore, C. Dolecek, M. Naghavi, Global burden of bacterial antimicrobial resistance in 2019: a systematic analysis. *The Lancet*. **399**, 629–655 (2022).

3. M. Lipsitch, M. H. Samore, Antimicrobial Use and Antimicrobial Resistance: A Population Perspective. *Emerg. Infect. Dis.* **8**, 347–354 (2002).

4. H. Goossens, M. Ferech, R. Vander Stichele, M. Elseviers, Outpatient antibiotic use in Europe and association with resistance: a cross-national database study. *The Lancet*. **365**, 579–587 (2005).

5. D. S. Sun, S. M. Kissler, S. Kanjilal, S. W. Olesen, M. Lipsitch, Y. H. Grad, Analysis of multiple bacterial species and antibiotic classes reveals large variation in the association between seasonal antibiotic use and resistance. *PLoS Biol.* **20**, e3001579 (2022).

6. S. W. Olesen, M. L. Barnett, D. R. MacFadden, J. S. Brownstein, S. Hernández-Díaz, M. Lipsitch, Y. H. Grad, The distribution of antibiotic use and its association with antibiotic resistance. *eLife*. **7**, e39435 (2018).

7. C. Tedijanto, S. W. Olesen, Y. H. Grad, M. Lipsitch, Estimating the proportion of bystander selection for antibiotic resistance among potentially pathogenic bacterial flora. *Proc. Natl. Acad. Sci.* **115**, E11988-E11995 (2018).

8. M. Stracy, O. Snitser, I. Yelin, Y. Amer, M. Parizade, R. Katz, G. Rimler, T. Wolf, E. Herzel, G. Koren, J. Kuint, B. Foxman, G. Chodick, V. Shalev, R. Kishony, Minimizing treatment-induced emergence of antibiotic resistance in bacterial infections. *Science*. **375**, 889–894 (2022).

9. D. R. Long, C. Bryson-Cahn, R. Pergamit, C. Tavolaro, R. Saigal, J. D. Chan, J. B. Lynch, 2021 Young Investigator Award Winner: Anatomic Gradients in the Microbiology of Spinal Fusion Surgical Site Infection and Resistance to Surgical Antimicrobial Prophylaxis. *Spine*. **46**, 143–151 (2021).

10. M. Hegreness, N. Shoresh, D. Damian, D. Hartl, R. Kishony, Accelerated evolution of resistance in multidrug environments. *Proc. Natl. Acad. Sci.* **105**, 13977–13981 (2008).

11. E. Toprak, A. Veres, J.-B. Michel, R. Chait, D. L. Hartl, R. Kishony, Evolutionary paths to antibiotic resistance under dynamically sustained drug selection. *Nat. Genet.* **44**, 101–105 (2012).

12. V. Lázár, G. Pal Singh, R. Spohn, I. Nagy, B. Horváth, M. Hrtyan, R. Busa-Fekete, B. Bogos, O. Méhi, B. Csörgő, G. Pósfai, G. Fekete, B. Szappanos, B. Kégl, B. Papp, C. Pál, Bacterial evolution of antibiotic hypersensitivity. *Mol. Syst. Biol.* **9**, 700 (2013).

13. M. Rodriguez de Evgrafov, H. Gumpert, C. Munck, T. T. Thomsen, M. O. A. Sommer, Collateral Resistance and Sensitivity Modulate Evolution of High-Level Resistance to Drug Combination Treatment in *Staphylococcus aureus*. *Mol. Biol. Evol.* **32**, 1175–1185 (2015).

14. L. Garoff, F. Pietsch, D. L. Huseby, T. Lilja, G. Brandis, D. Hughes, Population Bottlenecks Strongly Influence the Evolutionary Trajectory to Fluoroquinolone Resistance in *Escherichia coli*. *Mol. Biol. Evol.* **37**, 1637–1646 (2020).

15. N. Mahrt, A. Tietze, S. Künzel, S. Franzenburg, C. Barbosa, G. Jansen, H. Schulenburg, Bottleneck size and selection level reproducibly impact evolution of antibiotic resistance. *Nat. Ecol. Evol.* **5**, 1233–1242 (2021).

16. A. J. Lopatkin, S. C. Bening, A. L. Manson, J. M. Stokes, M. A. Kohanski, A. H. Badran, A. M. Earl, N. J. Cheney, J. H. Yang, J. J. Collins, Clinically relevant mutations in core metabolic genes confer antibiotic resistance. *Science*. **371**, eaba0862 (2021).

17. P. C. Münch, C. Eberl, S. Woelfel, D. Ring, A. Fritz, S. Herp, I. Lade, R. Geffers, E. A. Franzosa, C. Huttenhower, A. C. McHardy, B. Stecher, Pulsed antibiotic treatments of gnotobiotic mice manifest in complex bacterial community dynamics and resistance effects. *Cell Host Microbe*. **31**, 1007-1020.e4 (2023).

18. K. S. Vasquez, L. Willis, N. J. Cira, K. M. Ng, M. F. Pedro, A. Aranda-Díaz, M. Rajendram, F. B. Yu, S. K. Higginbottom, N. Neff, G. Sherlock, K. B. Xavier, S. R. Quake, J. L. Sonnenburg, B. H. Good, K. C. Huang, Quantifying rapid bacterial evolution and transmission within the mouse intestine. *Cell Host Microbe*. **29**, 1454-1468.e4 (2021).

19. J. C. Fung-Tomc, Correlation of in vitro and in vivo resistance development to antimicrobial agents. *Antimicrob. Newsl.* **7**, 17–24 (1990).

20. D. Hughes, D. I. Andersson, Evolutionary Trajectories to Antibiotic Resistance. *Annu. Rev. Microbiol.* **71**, 579–596 (2017).

21. L. J. Jahn, C. Munck, M. M. H. Ellabaan, M. O. A. Sommer, Adaptive Laboratory Evolution of Antibiotic Resistance Using Different Selection Regimes Lead to Similar Phenotypes and Genotypes. *Front. Microbiol.* **8**, 816 (2017).

22. D. A. Relman, M. Lipsitch, Microbiome as a tool and a target in the effort to address antimicrobial resistance. *Proc. Natl. Acad. Sci.* **115**, 12902–12910 (2018).

23. M. J. Bottery, J. W. Pitchford, V.-P. Friman, Ecology and evolution of antimicrobial resistance in bacterial communities. *ISME J.* **15**, 939–948 (2021).

24. A. J. Browne, M. G. Chipeta, G. Haines-Woodhouse, E. P. A. Kumaran, B. H. K. Hamadani, S. Zaraa, N. J. Henry, A. Deshpande, R. C. Reiner, N. P. J. Day, A. D. Lopez, S. Dunachie, C. E. Moore, A. Stergachis, S. I. Hay, C. Dolecek, Global antibiotic consumption and usage in humans, 2000–18: a spatial modelling study. *Lancet Planet. Health*. **5**, e893–e904 (2021).

25. D. Moradigaravand, M. Palm, A. Farewell, V. Mustonen, J. Warringer, L. Parts, Prediction of antibiotic resistance in Escherichia coli from large-scale pan-genome data. *PLoS Comput. Biol.* **14**, e1006258 (2018).

26. A. L. Hicks, N. Wheeler, L. Sánchez-Busó, J. L. Rakeman, S. R. Harris, Y. H. Grad, Evaluation of parameters affecting performance and reliability of machine learning-based antibiotic susceptibility testing from whole genome sequencing data. *PLoS Comput. Biol.* **15**, e1007349 (2019).

27. L. S. Redgrave, S. B. Sutton, M. A. Webber, L. J. V. Piddock, Fluoroquinolone resistance: mechanisms, impact on bacteria, and role in evolutionary success. *Trends Microbiol.* **22**, 438–445 (2014).

28. N. G. Bush, I. Diez-Santos, L. R. Abbott, A. Maxwell, Quinolones: Mechanism, Lethality and Their Contributions to Antibiotic Resistance. *Molecules*. **25**, 5662 (2020).

29. X. Li, N. Mariano, J. J. Rahal, C. M. Urban, K. Drlica, Quinolone-Resistant *Haemophilus influenzae* : Determination of Mutant Selection Window for Ciprofloxacin, Garenoxacin, Levofloxacin, and Moxifloxacin. *Antimicrob. Agents Chemother.* **48**, 4460–4462 (2004).

30. S. K. Morgan-Linnell, L. Zechiedrich, Contributions of the Combined Effects of Topoisomerase Mutations toward Fluoroquinolone Resistance in *Escherichia coli*. *Antimicrob. Agents Chemother.* **51**, 4205–4208 (2007).

31. D. L. Huseby, F. Pietsch, G. Brandis, L. Garoff, A. Tegehall, D. Hughes, Mutation supply and relative fitness shape the genotypes of ciprofloxacin-resistant *Escherichia coli*. *Mol. Biol. Evol.* **34**, 1029-1039 (2017).

32. S. Zhao, T. D. Lieberman, M. Poyet, K. M. Kauffman, S. M. Gibbons, M. Groussin, R. J. Xavier, E. J. Alm, Adaptive Evolution within Gut Microbiomes of Healthy People. *Cell Host Microbe*. **25**, 656-667.e8 (2019).

33. M. Poyet, M. Groussin, S. M. Gibbons, J. Avila-Pacheco, X. Jiang, S. M. Kearney, A. R. Perrotta, B. Berdy, S. Zhao, T. D. Lieberman, P. K. Swanson, M. Smith, S. Roesemann, J. E. Alexander, S. A. Rich, J. Livny, H. Vlamakis, C. Clish, K. Bullock, A. Deik, J. Scott, K. A. Pierce, R. J. Xavier, E. J. Alm, A library of human gut bacterial isolates paired with longitudinal multiomics data enables mechanistic microbiome research. *Nat. Med.* **25**, 1442–1452 (2019).

34. N. R. Garud, B. H. Good, O. Hallatschek, K. S. Pollard, Evolutionary dynamics of bacteria in the gut microbiome within and across hosts. *PLoS Biol.* **17**, e3000102 (2019).

35. E. Yaffe, D. A. Relman, Tracking microbial evolution in the human gut using Hi-C reveals extensive horizontal gene transfer, persistence and adaptation. *Nat. Microbiol.* **5**, 343–353 (2020).

36. M. Roodgar, B. H. Good, N. R. Garud, S. Martis, M. Avula, W. Zhou, S. M. Lancaster, H. Lee, A. Babveyh, S. Nesamoney, K. S. Pollard, M. P. Snyder, Longitudinal linked-read sequencing reveals ecological and evolutionary responses of a human gut microbiome during antibiotic treatment. *Genome Res.* **31**, 1433–1446 (2021).

37. S. Zlitni, A. Bishara, E. L. Moss, E. Tkachenko, J. B. Kang, R. N. Culver, T. M. Andermann, Z. Weng, C. Wood, C. Handy, H. P. Ji, S. Batzoglou, A. S. Bhatt, Strain-resolved microbiome sequencing reveals mobile elements that drive bacterial competition on a clinical timescale. *Genome Med.* **12**, 50 (2020).

38. D. W. Chen, N. R. Garud, Rapid evolution and strain turnover in the infant gut microbiome. *Genome Res.* **32**, 1124–1136 (2022).

39. S. Pecquet, S. Ravoire, A. Andremont, Faecal excretion of ciprofloxacin after a single oral dose and its effect on faecal bacteria in healthy volunteers. *J. Antimicrob. Chemother.* **26**, 125–129 (1990).

40. B. Fantin, X. Duval, L. Massias, L. Alavoine, F. Chau, S. Retout, A. Andremont, F. Mentré, Ciprofloxacin Dosage and Emergence of Resistance in Human Commensal Bacteria. *J. Infect. Dis.* **200**, 390–398 (2009).

41. L. Dethlefsen, D. A. Relman, Incomplete recovery and individualized responses of the human distal gut microbiota to repeated antibiotic perturbation. *Proc. Natl. Acad. Sci.* **108**, 4554–4561 (2011).

42. D. T. Truong, A. Tett, E. Pasolli, C. Huttenhower, N. Segata, Microbial strain-level population structure and genetic diversity from metagenomes. *Genome Res.* **27**, 626–638 (2017).

43. MetaHIT Consortium, H. B. Nielsen, M. Almeida, A. S. Juncker, S. Rasmussen, J. Li, S. Sunagawa, D. R. Plichta, L. Gautier, A. G. Pedersen, E. Le Chatelier, E. Pelletier, I. Bonde, T. Nielsen, C. Manichanh, M. Arumugam, J.-M. Batto, M. B. Quintanilha dos Santos, N. Blom, N. Borruel, K. S. Burgdorf, F. Boumezbeur, F. Casellas, J. Doré, P. Dworzynski, F. Guarner, T. Hansen, F. Hildebrand, R. S. Kaas, S. Kennedy, K. Kristiansen, J. R. Kultima, P. Léonard, F. Levenez, O. Lund, B. Moumen, D. Le Paslier, N. Pons, O. Pedersen, E. Prifti, J. Qin, J. Raes, S. Sørensen, J. Tap, S. Tims, D. W. Ussery, T. Yamada, P. Renault, T. Sicheritz-Ponten, P. Bork, J. Wang, S. Brunak, S. D. Ehrlich, Identification and assembly of genomes and genetic elements in complex metagenomic samples without using reference genomes. *Nat. Biotechnol.* **32**, 822–828 (2014).

44. S. Nayfach, Z. J. Shi, R. Seshadri, K. S. Pollard, N. C. Kyrpides, New insights from uncultivated genomes of the global human gut microbiome. *Nature*. **568**, 505–510 (2019).

45. J. N. Nissen, J. Johansen, R. L. Allesøe, C. K. Sønderby, J. J. A. Armenteros, C. H. Grønbech, L. J. Jensen, H. B. Nielsen, T. N. Petersen, O. Winther, S. Rasmussen, Improved metagenome binning and assembly using deep variational autoencoders. *Nat. Biotechnol.* **39**, 555-560 (2021).

46. C. Quince, T. O. Delmont, S. Raguideau, J. Alneberg, A. E. Darling, G. Collins, A. M. Eren, DESMAN: a new tool for de novo extraction of strains from metagenomes. *Genome Biol.* **18**, 181 (2017).

47. C. S. Smillie, J. Sauk, D. Gevers, J. Friedman, J. Sung, I. Youngster, E. L. Hohmann, C. Staley, A. Khoruts, M. J. Sadowsky, J. R. Allegretti, M. B. Smith, R. J. Xavier, E. J. Alm, Strain Tracking Reveals the Determinants of Bacterial Engraftment in the Human Gut Following Fecal Microbiota Transplantation. *Cell Host Microbe*. **23**, 229-240.e5 (2018).

48. C. Quince, S. Nurk, S. Raguideau, R. James, O. S. Soyer, J. K. Summers, A. Limasset, A. M. Eren, R. Chikhi, A. E. Darling, STRONG: metagenomics strain resolution on assembly graphs. *Genome Biol.* **22**, 214 (2021).

49. B. H. Good, M. M. Desai, Deleterious Passengers in Adapting Populations. *Genetics*. **198**, 1183–1208 (2014).

50. E. Orillard, M. Tan, Functional analysis of three topoisomerases that regulate DNA supercoiling levels in *Chlamydia*. *Mol. Microbiol.* **99**, 484–496 (2016).

51. J. Hirsch, D. Klostermeier, What makes a type IIA topoisomerase a gyrase or a Topo IV? *Nucleic Acids Res.* **49**, 6027–6042 (2021).

52. E. Helgesen, F. Sætre, K. Skarstad, Topoisomerase IV tracks behind the replication fork and the SeqA complex during DNA replication in *Escherichia coli*. *Sci. Rep.* **11**, 474 (2021).

53. X. Zhao, M. Malik, N. Chan, A. Drlica-Wagner, J.-Y. Wang, X. Li, K. Drlica, Lethal Action of Quinolones against a Temperature-Sensitive *dnaB* Replication Mutant of *Escherichia coli*. *Antimicrob. Agents Chemother.* **50**, 362–364 (2006).

54. D. H. Rubin, T. D. Mortimer, Y. H. Grad, *Neisseria gonorrhoeae* diagnostic escape from a gyrA-based test for ciprofloxacin susceptibility and the effect on zoliflodacin resistance: a bacterial genetics and experimental evolution study. *Lancet Microbe*. **4**, e247-e254 (2023).

55. O. M. Ghosh, B. H. Good, Emergent evolutionary forces in spatial models of luminal growth and their application to the human gut microbiota. *Proc. Natl. Acad. Sci.* **119**, e2114931119 (2022).

56. A. G. Kent, A. C. Vill, Q. Shi, M. J. Satlin, I. L. Brito, Widespread transfer of mobile antibiotic resistance genes within individual gut microbiomes revealed through bacterial Hi-C. *Nat. Commun.* **11**, 4379 (2020).

57. A. Bishara, E. L. Moss, M. Kolmogorov, A. E. Parada, Z. Weng, A. Sidow, A. E. Dekas, S. Batzoglou, A. S. Bhatt, High-quality genome sequences of uncultured microbes by assembly of read clouds. *Nat. Biotechnol.* **36**, 1067–1075 (2018).

58. Y. Suzuki, S. Nishijima, Y. Furuta, J. Yoshimura, W. Suda, K. Oshima, M. Hattori, S. Morishita, Long-read metagenomic exploration of extrachromosomal mobile genetic elements in the human gut. *Microbiome*. **7**, 119 (2019).

59. E. L. Moss, D. G. Maghini, A. S. Bhatt, Complete, closed bacterial genomes from microbiomes using nanopore sequencing. *Nat. Biotechnol.* **38**, 701–707 (2020).

60. N. J. Croucher, C. Chewapreecha, W. P. Hanage, S. R. Harris, L. McGee, M. Van Der Linden, J.-H. Song, K. S. Ko, H. De Lencastre, C. Turner, F. Yang, R. Sá-Leão, B. Beall, K. P. Klugman, J. Parkhill, P. Turner, S. D. Bentley, Evidence for Soft Selective Sweeps in the Evolution of Pneumococcal Multidrug Resistance and Vaccine Escape. *Genome Biol. Evol.* **6**, 1589–1602 (2014).

61. D. I. Andersson, D. Hughes, Antibiotic resistance and its cost: is it possible to reverse resistance? *Nat. Rev. Microbiol.* **8**, 260–271 (2010).

62. L. L. Marcusson, N. Frimodt-Møller, D. Hughes, Interplay in the Selection of Fluoroquinolone Resistance and Bacterial Fitness. *PLoS Pathog.* **5**, e1000541 (2009).

63. H. Yao, Z. Shen, Y. Wang, F. Deng, D. Liu, G. Naren, L. Dai, C.-C. Su, B. Wang, S. Wang, C. Wu, E. W. Yu, Q. Zhang, J. Shen, Emergence of a Potent Multidrug Efflux Pump Variant That Enhances *Campylobacter* Resistance to Multiple Antibiotics. *mBio*. **7**, e01543-16 (2016).

64. S. Baker, P. T. Duy, T. V. T. Nga, T. T. N. Dung, V. V. Phat, T. T. Chau, A. K. Turner, J. Farrar, M. F. Boni, Fitness benefits in fluoroquinolone-resistant *Salmonella* Typhi in the absence of antimicrobial pressure. *eLife*. **2**, e01229 (2013).

65. K. Davar, D. Clark, R. M. Centor, F. Dominguez, B. Ghanem, R. Lee, T. C. Lee, E. G. McDonald, M. C. Phillips, P. Sendi, B. Spellberg, Can the Future of ID Escape the Inertial Dogma of Its Past? The Exemplars of Shorter Is Better and Oral Is the New IV. *Open Forum Infect. Dis.* **10**, ofac706 (2023).

66. A. M. Bolger, M. Lohse, B. Usadel, Trimmomatic: a flexible trimmer for Illumina sequence data. *Bioinformatics*. **30**, 2114–2120 (2014).

67. R. Schmieder, R. Edwards, Fast Identification and Removal of Sequence Contamination from Genomic and Metagenomic Datasets. *PLoS ONE*. **6**, e17288 (2011).

68. D. Li, C. M. Liu, R. Luo, K. Sadakane, T. W. Lam, MEGAHIT: An ultra-fast single-node solution for large and complex metagenomics assembly via succinct de Bruijn graph. *Bioinformatics*. **31**, 1674–1676 (2014).

69. H. Li, R. Durbin, Fast and accurate short read alignment with Burrows-Wheeler transform. *Bioinforma. Oxf. Engl.* **25**, 1754–1760 (2009).

70. D. D. Kang, F. Li, E. S. Kirton, A. Thomas, R. S. Egan, H. An, Z. Wang, MetaBAT 2: an adaptive binning algorithm for robust and efficient genome reconstruction from metagenome assemblies. *PeerJ*. **7**, e7359 (2019).

71. D. R. Mende, I. Letunic, O. M. Maistrenko, T. S. B. Schmidt, A. Milanese, L. Paoli, A. Hernández-Plaza, A. N. Orakov, S. K. Forslund, S. Sunagawa, G. Zeller, J. Huerta-Cepas, L. P. Coelho, P. Bork, proGenomes2: an improved database for accurate and consistent habitat, taxonomic and functional annotations of prokaryotic genomes. *Nucleic Acids Res.* **48**, D621–D625 (2019).

72. D. H. Parks, M. Imelfort, C. T. Skennerton, P. Hugenholtz, G. W. Tyson, CheckM: assessing the quality of microbial genomes recovered from isolates, single cells, and metagenomes. *Genome Res.* **25**, 1043–1055 (2015).

73. P.-A. Chaumeil, A. J. Mussig, P. Hugenholtz, D. H. Parks, GTDB-Tk v2: memory friendly classification with the genome taxonomy database. *Bioinformatics*. **38**, 5315–5316 (2022).

74. K. P. Schliep, phangorn: phylogenetic analysis in R. *Bioinformatics*. **27**, 592–593 (2011).

75. D. Hyatt, G.-L. Chen, P. F. LoCascio, M. L. Land, F. W. Larimer, L. J. Hauser, Prodigal: prokaryotic gene recognition and translation initiation site identification. *BMC Bioinformatics*. **11**, 119 (2010).

76. B. Buchfink, C. Xie, D. H. Huson, Fast and sensitive protein alignment using DIAMOND. *Nat. Methods*. **12**, 59–60 (2015).

77. M. Steinegger, J. Söding, MMseqs2 enables sensitive protein sequence searching for the analysis of massive data sets. *Nat. Biotechnol.* **35**, 1026–1028 (2017).

78. J. Huerta-Cepas, D. Szklarczyk, D. Heller, A. Hernández-Plaza, S. K. Forslund, H. Cook, D. R. Mende, I. Letunic, T. Rattei, L. J. Jensen, C. von Mering, P. Bork, eggNOG 5.0: a hierarchical, functionally and phylogenetically annotated orthology resource based on 5090 organisms and 2502 viruses. *Nucleic Acids Res.* **47**, D309–D314 (2019).

79. F. Sievers, A. Wilm, D. Dineen, T. J. Gibson, K. Karplus, W. Li, R. Lopez, H. McWilliam, M. Remmert, J. Söding, J. D. Thompson, D. G. Higgins, Fast, scalable generation of high-quality protein multiple sequence alignments using Clustal Omega. *Mol. Syst. Biol.* **7**, 539 (2011).

80. D. L. Hartl, A. G. Clark, *Principles of population genetics* (Sinauer Associates, Sunderland, Mass, 4th ed., 2007).

81. Gillespie, J.H., *Population Genetics: A Concise Guide.* (Johns Hopkins University Press, 2004).

ACKNOWLEDGMENTS

We extend our gratitude to Benjamin Good and Elizabeth Costello (Stanford University) for their valuable insights and constructive feedback.

FUNDING

This work was funded by the National Institute of Allergy and Infectious Diseases of the National Institutes of Health (grant R01AI147023) and the Thomas C. and Joan M. Merigan Endowment at Stanford University.

COMPETING INTERESTS

The authors declare that they have no conflict of interest.

DATA AVAILABILITY

The source code for PolyPanner is available at https://github.com/eitanyaffe/PolyPanner. Unprocessed DNA sequence reads will be made available upon publication in the NCBI database, under project PRJNA974858.

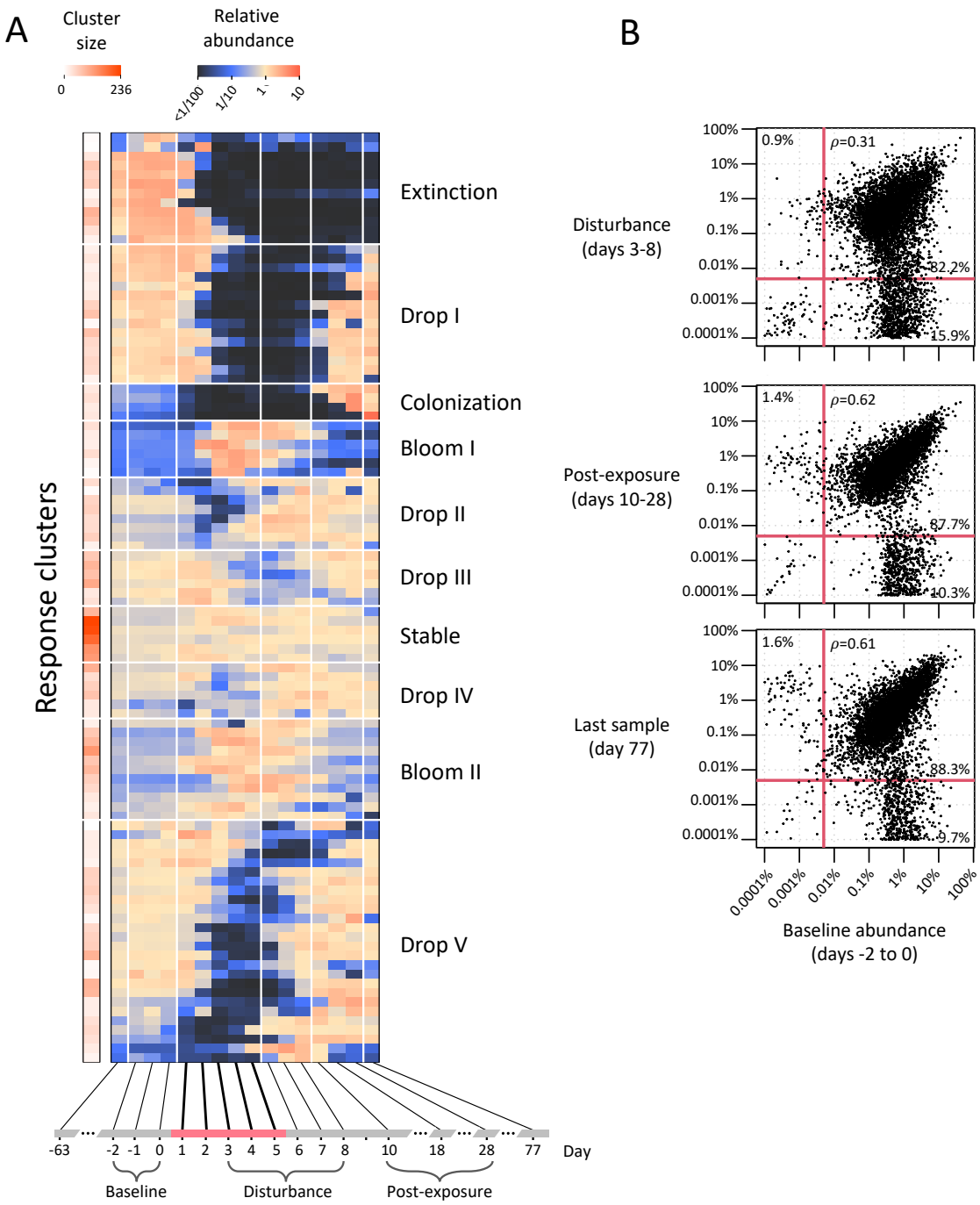

Fig. 1. Population-level responses to ciprofloxacin. A) Abundance trajectories of all 5665 metagenome-assembled genomes (MAGs) were each normalized relative to their respective mean and clustered using k-means into 100 response clusters or trends. Trends are organized vertically using hierarchical clustering, with the number of populations per cluster shown by a color bar on the left. The mean-centered abundance of each cluster across 16 temporal samples is shown horizontally, with ciprofloxacin course days indicated in red along the axis (shifted by a

day to reflect transit time). **B)** Scatter plots comparing the baseline pre-exposure population abundances to three later timeframes. Each scatter plot depicts for each population the baseline abundance (x-axis, average of days -2 to 0) vs. one of three timeframes (during the height of disturbance at days 3-8, post exposure at days 10-28, and on the last day of sampling, day 77). A pseudo count of 0.0001% was added to each count for visualization purposes. Vertical/horizontal red lines represent a detection threshold of 0.005%. The percentages of populations within quadrants are shown, as are Spearman correlation coefficients between populations detected in both timeframes.

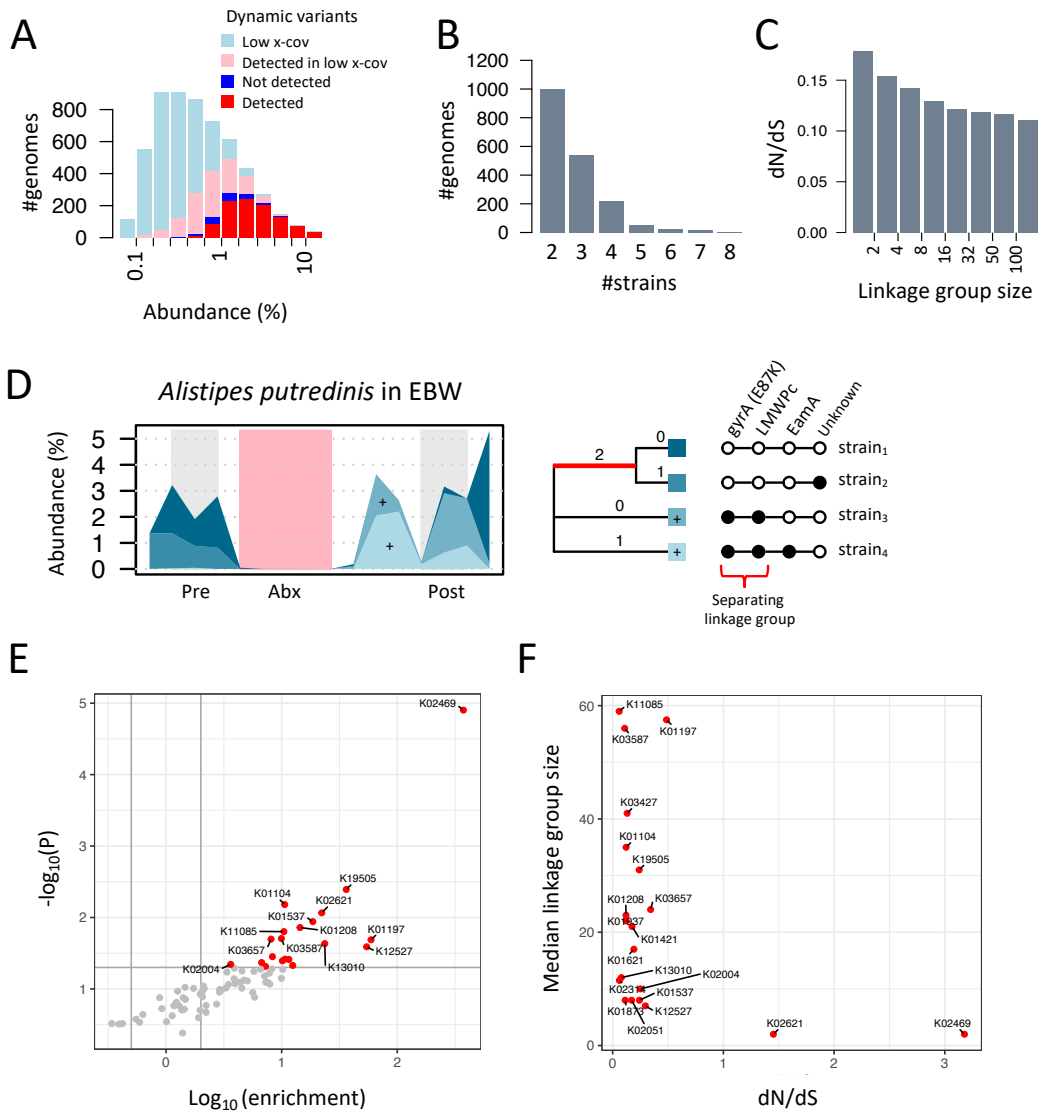

Fig 2. Variants, strains, linkage groups and converging evolution analysis. A) Number of population genomes (y-axis) as a function of the average population abundance (x-axis). Colors denote four population types: 1018 populations with dynamic variants and sufficient x-coverage to detect sweeps if present (red, "Detected"), 168 populations with no dynamic variants and sufficient x-coverage (dark blue, "Not detected"), 1115 populations with dynamic variants and low x-coverage (pink, "Detected in low x-cov"), and 3364 populations with no variants and low x-coverage (light blue, "Low x-cov"). **B)** Number of genomes containing dynamic variants (y-axis) as a function of the number of inferred strains (x-axis). **C)** dN/dS ratios (y-axis) as a function of the linkage group (LG) size (x-axis). **D)** Temporal dynamics of the population of *Alistipes putredinis* in subject EBW. On the right is the variant-strain matrix, with 4 bi-allelic polymorphic loci (columns, named according to gene), and 4 strains (rows), with black and white circles depicting

the variants present in a strain. The strain phylogeny (generated through maximum parsimony) is shown in the middle, with the number of switching variants displayed above each edge. The edge associated with the linkage group that separates strains 1+2 from strains 3+4 is colored in red. Shown on the left is the temporal abundance of strains (strains stacked) over the 16 temporal samples (x-axis), with background colors emphasizing pre (antibiotic) samples (days -2 to 0, gray), disturbed samples (days 3-8, pink) and post (antibiotic) samples (days 10-28, gray). Plus signs denote strains 3 and 4, which become the dominant strains after the exposure. Strain order and representation as shades of blue are consistent across the panel. **E)** Variants were assigned weights equal to the inverse of their smallest linkage group, weights were aggregated within KEGG Orthology annotations (KOs) of associated genes and then compared to a null model of weights across KOs generated through permutations. A volcano plot depicts weight enrichment ratios over the null model (x-axis) vs. P-values (y-axis). Significant KOs ($P<0.05$) are colored red. K02469 is *gyrA* and K02621 is *parC*, other KO descriptions are given in **Supp. Figure S12**. **F)** For each significant KO, the dN/dS ratio (x-axis) of the supporting variants is plotted vs. the median linkage group size of the supporting variants (y-axis).

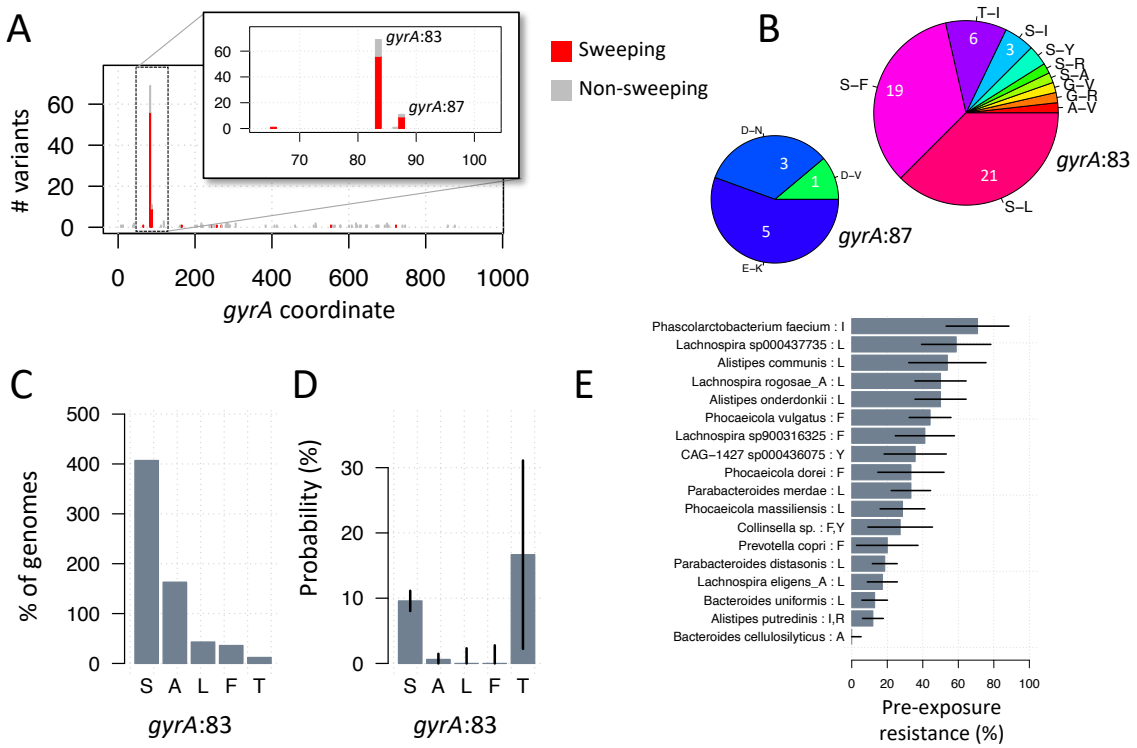

Fig. 3. Focused selective pressure on *gyrA*. A) The number of variants (y-axis) for each amino acid (AA) position within the *gyrA* gene (x-axis, *E. coli* numbering). Sweeping and non-sweeping variant counts are colored red and gray respectively. **B)** Breakdown of substitutions associated with sweeping variants at *gyrA*:83 and *gyrA*:87, letters represent amino acids (e.g., 'S-F' represents a substitution of serine by phenylalanine). **C)** Breakdown of all genomes containing *gyrA* according to the baseline AA identity at *gyrA*:83 before the exposure. **D)** Exposure-associated substitution probability, stratified by the baseline AA at *gyrA*:83. Confidence intervals showing the standard deviation depicted with vertical lines. **E)** Species-specific resistance alleles at *gyrA*:83 were determined for 31 species based on observed exposure-associated substitutions. The percentage of resistance alleles prior to exposure is shown for 18 species represented by at least 10 populations. Resistance alleles are shown next to the species name. For example, *Alistipes putredinis* has two resistance alleles at *gyrA*:83, namely isoleucine ('I') and arginine ('R'), and 12% (5/42) of *A. putredinis* populations had either of these alleles prior to the exposure. Black bars represent standard deviation estimates.

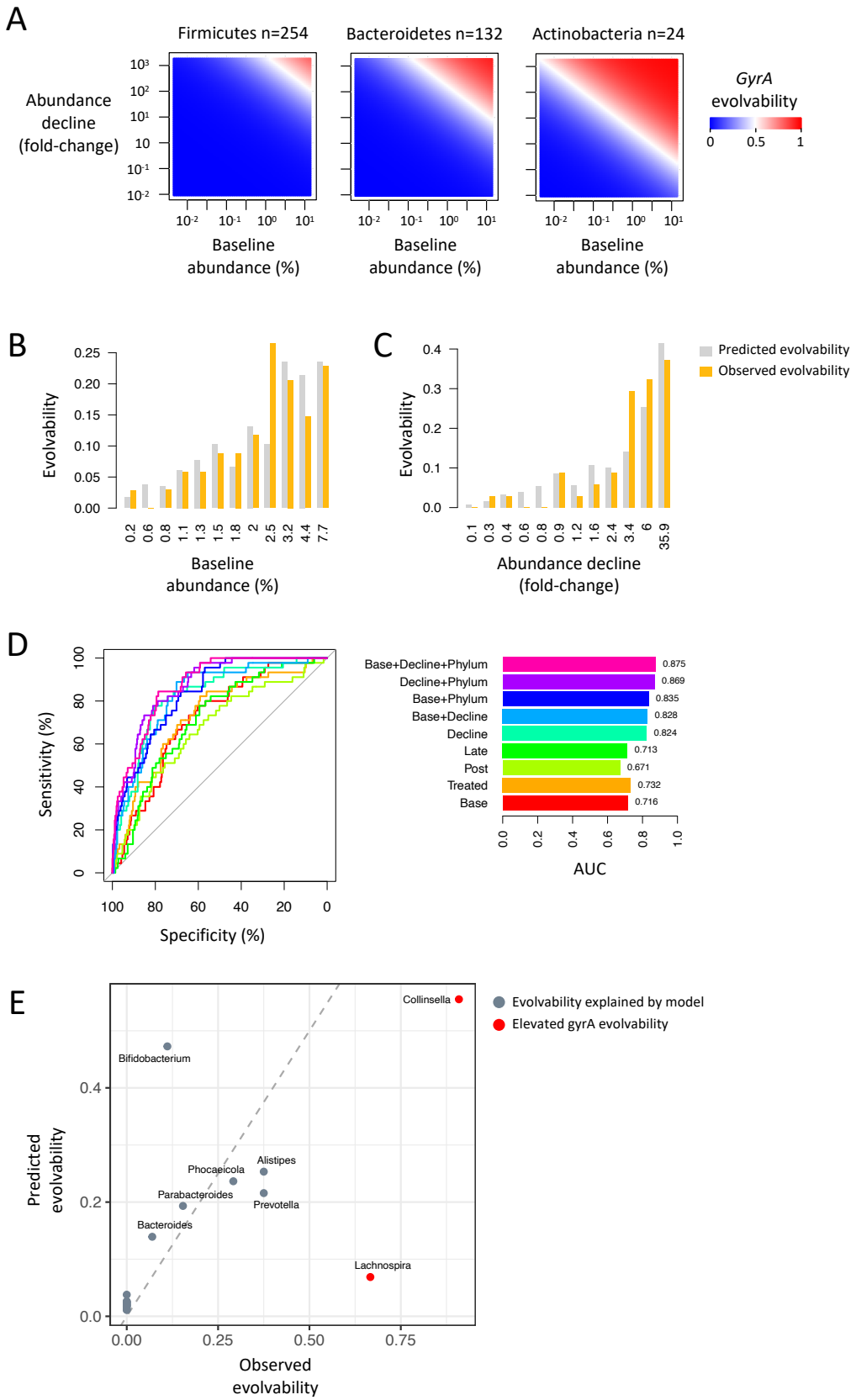
A
Firmicutes n=254
Bacteroidetes n=132
Actinobacteria n=24
Abundance decline (fold-change)
Baseline abundance (%)
GyrA evolvability
B
Evolvability
Baseline abundance (%)
C
Evolvability
Abundance decline (fold-change)
Predicted evolvability
Observed evolvability
D
Sensitivity (%)
Specificity (%)
Base+Decline+Phylum 0.875
Decline+Phylum 0.869
Base+Phylum 0.835
Base+Decline 0.828
Decline 0.824
Late 0.713
Post 0.671
Treated 0.732
Base 0.716
AUC
E
Collinsella
Bifidobacterium
Phocaeicola
Alistipes
Parabacteroides
Prevotella
Bacteroides
Lachnospira
Predicted evolvability
Observed evolvability
Evolvability explained by model
Elevated gyrA evolvability

Fig. 4. Abundance-dependent evolution of antibiotic resistance. A) *GyrA* evolvability as predicted by a fitted logistic regression model based on variables for the baseline population abundance (average of days -2 to 0, x-axis), the fold-change decline during antibiotics (average of days 1-5, y-axis), and phylum (separate plot for each of three phyla). **B)** Model-predicted and observed *gyrA* evolvability (y-axis) as a function of baseline abundances. **C)** Model-predicted and observed *gyrA* evolvability (y-axis) as a function of the fold-change decline in population abundances during antibiotics (days 1-5). **D)** Shown on left are ROC curves (receiver operating characteristic curves) of 9 inferred logistic regression models that predict the probability of a population to have a sweeping *gyrA* variant. Shown on right are the areas under the curve (AUC) of all models. **E)** Observed (x-axis) vs. model-predicted (y-axis) genus-level *gyrA* evolvability, for the 21 genera associated with at least 6 populations. Genera are colored red if differences between observed and predicted evolvability were significant (Binomial distribution, $P<0.05$), and colored gray otherwise. Dashed line depicts the line x=y.

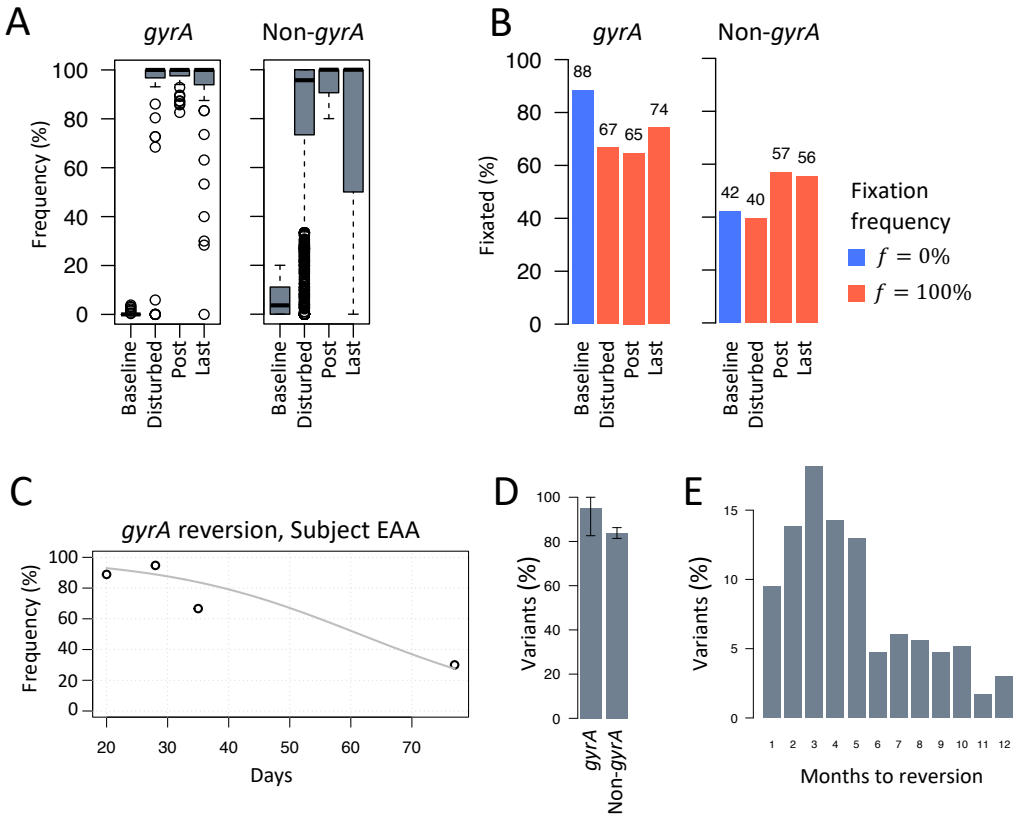

Fig. 5. Long-term persistence of antibiotic-associated genetic changes. A) Boxplots depicting the distribution of the frequencies of sweeping *gyrA* variants (left) and non-*gyrA* variants (right), stratified by time windows (day ranges defined in panel 1A). Gray rectangles span the first and third quartiles, horizontal line depicts the median, dashed line spans between the 5th and the 95th percentiles, and outliers outside that range are plotted as circles. **B)** The percentage of sweeping variants fixated at 0% frequency at baseline (blue) or fixated at 100% within the 3 other time windows (red), shown separately for *gyrA* variants (left) and non-*gyrA* variants (right). **C)** Example of a sweeping *gyrA* variant in subject EAA that was projected to revert below a frequency of 1% within 135 days. Circles depict the variant frequency (y-axis) as a function of the day relative to the start of the antibiotics (x-axis). Gray line shows an exponential decay, based on a constant selection coefficient of 0.006 that was inferred from the temporal frequency data, assuming 10 generations per day. **D)** The percentage of sweeping *gyrA* variants (left) and sweeping non-*gyrA* variants (right) that were projected to require more than a year to revert below a frequency of 1%. Vertical lines depict estimates of the standard deviation. **E)** For sweeping variants that were projected to fall below a frequency of 1% within a year, a histogram of the number of months until reversion.